Available online at www.sciencedirect.com

SciVerse ScienceDirect

Ceramics International 38 (2012) 3343–3350

CERAMICS INTERNATIONAL

www.elsevier.com/locate/ceramint

# Synthesis and characterization of dense and fine nickel ferrite ceramics through two-step sintering

Zhigang Zhang, Yihan Liu, Guangchun Yao *, Guoyin Zu, Di Wu, Yi Hao

*Advanced Manufacturing Technology and Engineering Research Centers, School of Materials and Metallurgy, Northeastern University, Shenyang 110819, PR China*

Received 15 November 2011; received in revised form 17 December 2011; accepted 17 December 2011
Available online 27 December 2011

**Abstract**

Two-step sintering (TSS) has been employed in the current study to suppress the accelerated grain growth of $NiFe_2O_4$ nanopowder compacts in the final sintering stage. Experiments are conducted to determine the appropriate temperatures for each step. The temperature range from 1200 °C to 1300 °C is effective for the first-step sintering ($T_1$) due to its highest densification rate. The second-step sintering temperature ($T_2$) should be within the kinetic window, where grain boundary diffusion is maintained but grain boundary migration is suppressed. The grain sizes of high density (≥98% theoretical density) $NiFe_2O_4$ compacts produced by TSS are smaller than 700 nm, while that of those formed by CS are over 2.5 μm. The evidence indicates that the saturation magnetization of nearly full $NiFe_2O_4$ ceramics is independent of grain size and likewise high, with the corresponding values of approximately 54 emu/g. The Vickers hardness and fracture toughness both increase with the decrease of grain size and porosity.



*Keywords:* A. Sintering; B. Grain size; C. Magnetic properties; C. Mechanical properties; D. Ferrites

## 1. Introduction

The outstanding attention has recently been devoted to full dense ceramics with fine grain size, originating from advantages of their unusual mechanical, optical and magnetic properties [1–5]. Substantial research has been done on reducing grain size to below 1 μm as well as reaching near full density, aiming to quest for these promising functional and structural properties. In the production process of ceramics, sintering is the most significant procedure whereby interparticle pores in a granular material are eliminated by atomic diffusion driven by capillary forces [6]. Accordingly, sintering methods play a major role in developing high density ceramics with fine grain size. As various sintering methods proceed through diverse mechanisms and densification kinetics, it is possible to acquire sintered ceramics with desired microstructure. Several sintering methods including conventional sintering (CS), spark plasma sintering (SPS), hot isostatic pressing sintering (HIP) and microwave sintering (MW) have already been employed to obtain nearly full dense ceramics [7–14]. Conventional pressureless sintering is the most common low-cost approach to sinter ceramics. Unfortunately, it is difficult to realize densification without promoting grain growth, because both processes of densification and grain growth are driven by diffusion. Pressure-assisted methods such as SPS and HIP and microwave sintering yield a rapid sintering rate, high density and ultrafine grain structure. However, the limitations such as high production cost, sophisticated equipment and shape complexity make these hardly accessible and scarcely useful for practical applications. Consequently, there is still a need for an alternative technique for producing fully dense ceramics with fine grain size in a simple way.

Chen and Wang [6] have developed an effective pressureless method called two-step sintering (TSS) for the sintering of $Y_2O_3$. The $Y_2O_3$ nanopowder compacts are first heated to a higher temperature ($T_1$) so as to achieve an intermediate density, then cooled down rapidly and held at a lower temperature ($T_2$) until there are fully dense. By this method, the grain boundary diffusion is maintained but the grain boundary migration could be frozen under pressureless

* Corresponding author. Tel.: +86 24 83686462; fax: +86 24 83682912.
*E-mail addresses:* gangzi2323@126.com (Z. Zhang), gcyao@mail.neu.edu.cn (G. Yao).

0272-8842/$36.00. 
doi:10.1016/j.ceramint.2011.12.044

conditions. Therefore, the grain growth in the final sintering stage is suppressed successfully to obtain full dense $Y_2O_3$ ceramics with nano-grains. The key elements in this method reported by Chen and colleagues [6,15,16] are (a) reaching a higher temperature ($T_1$) to conduct the first-step sintering, (b) achieving a critical density of $\rho^* \geq 75\%$ theoretical density (TD) to render pores unstable, and (c) lowering the temperature to $T_2$ to conduct the second-step sintering during which there is only densification and no grain growth. In addition to $Y_2O_3$, such TSS method has been successfully utilized for the sintering of $BaTiO_3$ [16,17], Ni–Cu–Zn ferrite [16], ZnO [18,19], 3Y-TZP [20], $Al_2O_3$ [21], $TiO_2$ [22] and SiC [23].

$NiFe_2O_4$ is an attractive material usable in such applications as high-density magnetic recording, magnetic fluids, microwave absorbents, pigments, biomedical and clinical devices, gas sensors, electronic devices and catalytic materials [24,25]. Furthermore, nickel ferrite matrix ceramic inert anode becomes a preferred material for aluminum electrolysis for its high corrosion resistance and high electrochemical stability in molten cryolite-alumina [26,27]. These and other prospective applications have, in recent years, led to growing interest in the processing of nickel ferrite bulk ceramics. Most reports on the fabrication of $NiFe_2O_4$ ceramics have been conducted by conventional pressureless sintering, therefore, abnormal grain growth could occur with ease. The brittle $NiFe_2O_4$ ceramics consisting of coarse grains as well as high porosity possess poor fracture resistance and toughness, resulting to catastrophic fracture easy as can. Hence, that limits their further structural and functional applications. It is well-known that grain refining as well as porosity decreasing is a promising route for simultaneous increase of mechanical strength and fracture toughness. Consequently, the need for high density $NiFe_2O_4$ ceramics with fine grain size has still not been satisfied radically. So far, there are no published reports on fabrication of high density $NiFe_2O_4$ ceramics with fine grain size by means of TSS.

In this work, $NiFe_2O_4$ spinel nanopowder was synthesized by a solid-state reaction route. Then the nanopowder compacts were conducted by CS and TSS. CS and different TSS regimes were designed to analyze the effects of $T_1$ and $T_2$ on the density and grain size of obtained ceramics. High density $NiFe_2O_4$ ceramics with fine grain size were obtained by a properly designed TSS regime in this research. The magnetic and mechanical properties of $NiFe_2O_4$ ceramics prepared under various conditions were also investigated in details.

## 2. Experimental procedures

### 2.1. Nanopowder preparation

The $NiFe_2O_4$ spinel nanopowder was synthesized by a solid-state reaction route using ferrous sulfate heptahydrate ($FeSO_4{\cdot}7H_2O$), nickel (II) sulfate hexahydrate ($NiSO_4{\cdot}6H_2O$) and sodium hydroxide (NaOH) as reactants and sodium chloride (NaCl) as dispersant. The precursor was prepared by adequately grinding the mixture, comprising reactants of calculated proportion and 20 wt% NaCl, in an agate mortar for about 15 min at ambient temperature. After calcining the precursor in air at 800 °C for 1 h, $NiFe_2O_4$ nanopowder was obtained by washing away NaCl and $Na_2SO_4$ salts and unreacted reagents thoroughly with distilled water.

### 2.2. Sample compaction and sintering

The powder was uniaxially cold pressed at 300 MPa into pellets with a diameter of 10.1 mm and a thickness of 3 mm. Based on the $NiFe_2O_4$ theoretical density of 5.37 g/cm$^3$, the average green density of the $NiFe_2O_4$ nanopowder compacts was determined to be ~0.56 TD after pressing. Sintering of the green bodies was carried out by conventional sintering and two-step sintering methods. CS was carried out at 1000–1400 °C in air with 50 °C temperature intervals and a heating ramp of 10 °C/min. The specimens were heated up to the highest temperature without any holding time and then cooled down to room temperature naturally in the furnace. In order to determine the $T_1$ for the first-step of TSS, the nanopowder compact was heated with 10 °C/min from room temperature to 1400 °C without any holding time and then cooled down to room temperature, while the linear shrinkage data was simultaneously recorded by a dilatometer (DIL 402 PC, NETZSCH, Germany). The linear shrinkage rate was obtained by differentiating the measured linear shrinkage. In two-step sintering, the samples were first heated at 10 °C/min to a higher temperature $T_1$, then immediately cooled at 30 °C/min to a lower temperature $T_2$ and held there for isothermal sintering with a dwelling time of 10–20 h.

### 2.3. Characterization

The as-synthesized nanopowder was characterized by X-ray diffraction (XRD) (Model X' Pert Pro, PANalytical, Netherlands) and transmission electron microscopy (TEM) (Model Tecnai G$^2$20, FEI, USA). The average crystallite size ($D$) of the $NiFe_2O_4$ particles was estimated from the full width at half maximum (FWHM) of the most intense diffraction line (3 1 1) using the well-known Scherrer's equation [28]:

$$D = \frac{0.89\lambda}{\beta \cos\theta} \quad (1)$$

where $\lambda = 0.154060$ nm, the wave length of Cu Kα, $\beta$ is the broadening of diffraction line measured at half maximum intensity (radians) and $\theta$ is the Bragg's angle.

For microstructural characterization, the sintered pellets were first fractured and then studied using scanning electron microscopy (SEM) (Model SSX-550, SHIMADZU, Japan). An image analyzer calculated the mean grain size of the samples. The densities of the sintered bulks were determined using Archimedes' method with deionized water as the immersion medium. At least three samples were used to determine the average grain size and density corresponding to each data point.

Magnetic properties of $NiFe_2O_4$ ceramics prepared by various conditions were measured at room temperature using vibrating sample magnetometer (VSM) (Model 7407, Lake

Shore, USA) with an applied field of ±10 kOe. For the VSM test, the samples were processed from cylinder to cuboid with the dimensions of 3 mm × 3 mm × 2 mm.

Vickers hardness and fracture toughness were carried out by indentation method using Vickers hardness tester (450SVD, TMS, China). Indentation test was conducted on polished samples with a load of 10 kg held for 20 s at ambient conditions. The length of each diagonal of the square shaped Vickers indentation and crack length emanating the indentation center were measured by SEM under secondary electron imaging. The Vickers hardness ($H_v$) was calculated from the diagonal length of the indentation using the standard Vickers formula [29]:

$$H_v = 1.8544\frac{P}{d^2} \quad (2)$$

where $P$ is the applied indentation load and $d$ is the mean value of the diagonal length of the indentation. The resultant crack length for each indentation has been estimated by taking the average of all the crack lengths produced due to the indentation and hence fracture toughness ($K_{IC}$) was calculated from the following equation [30]:

$$K_{IC} = 0.016\left(\frac{E}{H_v}\right)^{1/2}\left(\frac{P}{C^{3/2}}\right) \quad (3)$$

where $E$ is the Young's modulus, $H_v$ is the Vickers hardness, $P$ is the applied indentation load and $C$ is the average crack length emanating the indentation center.

## 3. Results and discussion

### 3.1. Nanopowder characterization

Fig. 1 shows the morphology of the $NiFe_2O_4$ nanopowder calcined at 800 °C for 1 h. It can be observed that the particles have a size range of 30–40 nm and a mostly polyhedral shape. The diffractogram plotted in Fig. 2 presents the XRD pattern of

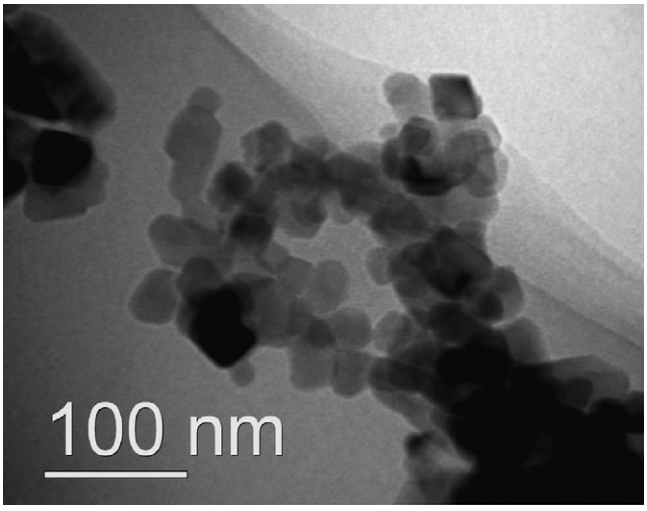


Fig. 1. TEM micrograph of as-synthesized $NiFe_2O_4$ nanopowder.

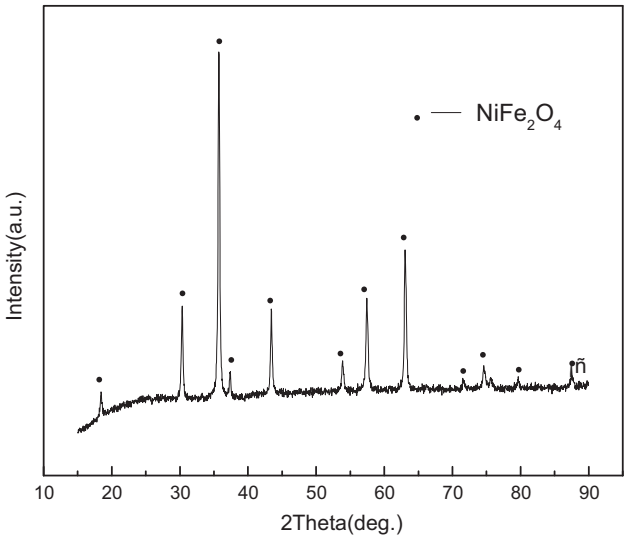


Fig. 2. XRD pattern of as-synthesized $NiFe_2O_4$ nanopowder.

the $NiFe_2O_4$ nanopowder. All the diffraction peaks match perfectly with the standard JCPDS data 01-086-2267, which is the nickel ferrite card. The average crystallite size of the $NiFe_2O_4$ nanopowder is determined to be 41 nm by means of Scherrer's equation (Eq. (1)), which is consistent with the result of TEM.

### 3.2. Conventional sintering

The variations in relative density and grain size of conventional sintered samples with sintering temperature are sketched in Fig. 3. The relative density versus temperature plot exhibits a slight sigmoidal shape in the temperature range of 1000–1400 °C while the grain size displays an upward concave curve. No significant densification and grain growth are observed below 1050 °C. The sintering rate increases approximately linearly between 1100 °C and 1300 °C, resulting in the relative density changing from 69.84%TD to 89.89%TD and the average grain size increasing from 144 nm to 634 nm.

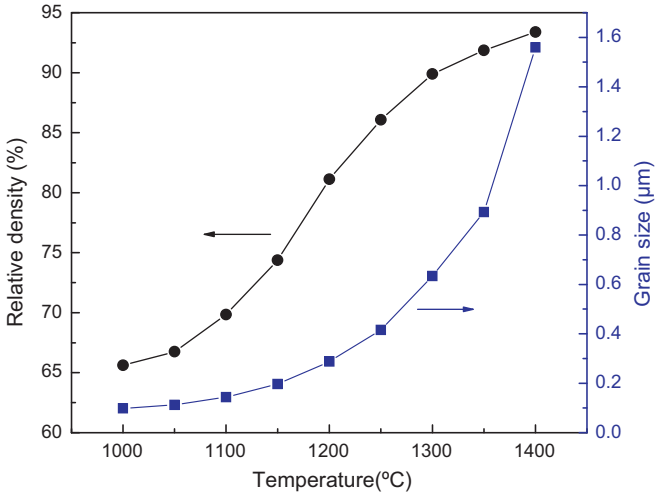


Fig. 3. Relative density and grain size of conventionally sintered $NiFe_2O_4$ compacts as a function of sintering temperature.

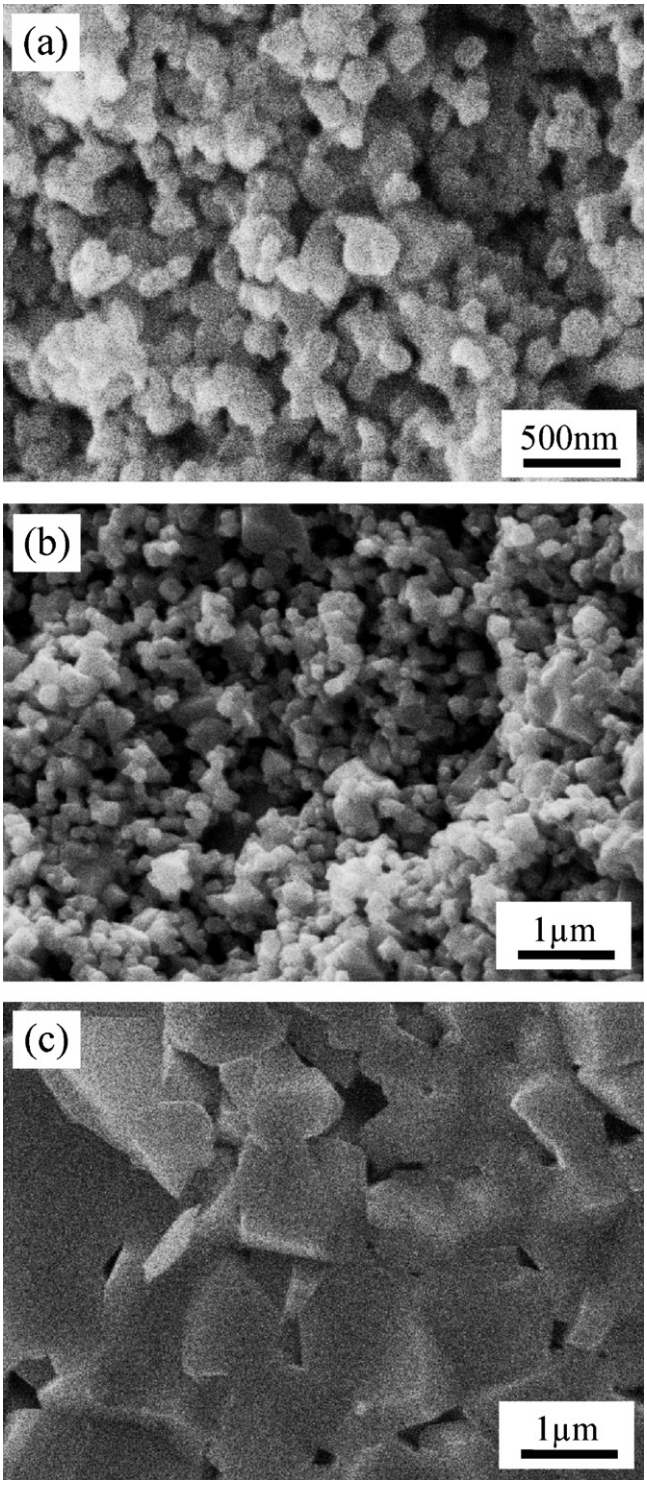


Fig. 4. SEM micrographs of conventional sintered specimens at (a) 1050 °C, (b) 1250 °C, and (c) 1400 °C without any holding time, respectively.

Further increase in temperature (from 1300 °C to 1400 °C) leads to a slight strengthening in density (up to 3.51%) whereas a remarkable increase in grain size (1.56 μm at 1400 °C). Since both densification and grain growth are aroused by diffusion, whose mechanisms are dependent on temperature, the temperature increases will clearly enhance a simultaneous advance in density and grain size [22]. However, the pronounced effects on density and grain size by temperature increase are various at different sintering stages. Fig. 4 shows SEM micrographs of conventional sintered specimens at (a) 1050 °C, (b) 1250 °C, and (c) 1400 °C without any holding time, respectively. When the temperature falls below 1100 °C, only the initial stage of sintering occurs, where the granules adhere and sintering necks are formed, as presented in Fig. 4(a). As the temperature increases, sintering necks grow and the connected network of pores (as shown in Fig. 4(b)) is formed, which exists throughout the second stage of sintering. The pore pinning phenomenon, according to which the grain boundaries are dragged by the existing connected network of pores, is responsible for the continuous densification without noteworthy grain growth [22]. With the beginning of the final stage of sintering, however, the abovementioned connected network of pores disintegrates and open pores collapse to the closed ones. Such a situation induces an adequate movement of grain boundaries and therefore a predicable remarkable grain growth [18]. This is verified by Fig. 4(c), in which the pores become independent and the grains grow dramatically. Consequently, the grain growth eventually dominates above 1300 °C and leads to a disapproved microstructural coarsening.

### 3.3. Two-step sintering

According to Chen and Wang [6], the success of two-step sintering forcefully depends on the choices of temperatures $T_1$ and $T_2$. Based on the key elements for TSS aforementioned, the intermediate density after the first-step sintering of TSS ($T_1$) should be higher than 75%TD, corresponding to a state in which all pores are unstable and shrinkable. Fig. 5 shows the linear shrinkage rate as a function of temperature. It reveals that the linear shrinkage rate, identifying with densification rate, increases with the sintering temperature to a plateau in the range of 1200–1300 °C and the decreases sharply from 1300 °C to 1400 °C. Based on Hansen et al.'s sintering model [31], the exhaustion of densification rate is associated with the final

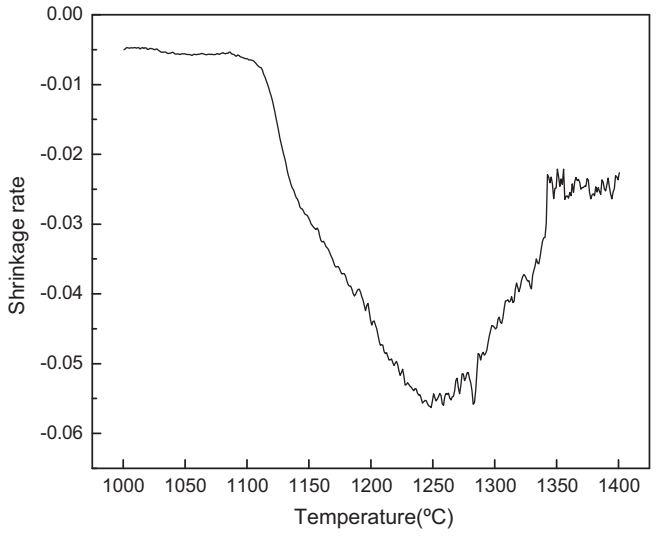


Fig. 5. Shrinkage rate against temperature for constant-heating-rate sintering.

Table 1
Relative densities and grain sizes of $NiFe_2O_4$ specimens under various heating parameters of two-step sintering.

| Sample | $\rho_0$ (%) | After first-step sintering | | | | After second-step sintering | | | |
|---|---|---|---|---|---|---|---|---|---|
| | | $T_1$ (°C) | $t_1$ (h) | $\rho_1$ (%) | $G_1$ (nm) | $T_2$ (°C) | $t_2$ (h) | $\rho_2$ (%) | $G_2$ (nm) |
| 1 | 56 | 1200 | 0 | 81.13 | 288 | 1100 | 10 | 98.21 | 290 |
| 2 | 56 | 1200 | 0 | 81.13 | 288 | 1100 | 15 | 99.10 | 290 |
| 3 | 56 | 1200 | 0 | 81.13 | 288 | 1100 | 20 | 99.12 | 290 |
| 4 | 56 | 1200 | 0 | 81.13 | 288 | 1125 | 15 | 99.41 | 295 |
| 5 | 56 | 1250 | 0 | 86.07 | 416 | 1100 | 15 | 98.67 | 420 |
| 6 | 56 | 1250 | 0 | 86.07 | 416 | 1125 | 15 | 99.31 | 420 |
| 7 | 56 | 1250 | 0 | 86.07 | 416 | 1150 | 15 | 99.52 | 430 |
| 8 | 56 | 1275 | 0 | 87.88 | 492 | 1100 | 15 | 98.40 | 495 |
| 9 | 56 | 1275 | 0 | 87.88 | 492 | 1125 | 15 | 99.12 | 495 |
| 10 | 56 | 1275 | 0 | 87.88 | 492 | 1150 | 15 | 99.61 | 500 |
| 11 | 56 | 1300 | 0 | 89.89 | 634 | 1075 | 15 | 98.01 | 635 |
| 12 | 56 | 1300 | 0 | 89.89 | 634 | 1100 | 15 | 98.32 | 635 |
| 13 | 56 | 1300 | 0 | 89.89 | 634 | 1125 | 15 | 98.51 | 635 |
| 14 | 56 | 1300 | 0 | 89.89 | 634 | 1150 | 15 | 99.12 | 640 |
| 15 | 56 | 1300 | 0 | 89.89 | 634 | 1175 | 15 | 99.61 | 640 |

sintering stage or grain coarsening. According to Fig. 3, when the sintering temperature is over 1300 °C, an obvious grain growth is observed corresponding to the decrease of linear shrinkage rate. As the state of the specimen after the first step sintering critically affects the subsequent second step and the final grain size of sintered specimens, the grain growth resulted from over-heating in the first step should be as little as possible. Therefore, the appropriate temperature $T_1$ is set at the range of 1200–1300 °C where the corresponding relative density is from 81.13% to 89.89% and grain size is from 288 nm to 634 nm.

With regard to the determination of $T_2$ for the second-step of TSS, previous researches [6,15,16] have reported that it should be restricted within a range, called the kinetic window, where grain boundary diffusion needs to be maintained while grain boundary migration is suppressed. It is worth noting that the choice of $T_2$ is extremely considerable because the undesired grain growth may be generated when the $T_2$ is higher; in contrary, an incomplete densification is attained owing to the insufficiency of grain boundary diffusion. Previous successful experiences for TSS exhibit that the $T_2$ should be lower than $T_1$ with a gap of 50–150 °C [6,15,16,18]. In this study, various TSS regimes with different $T_1$ and $T_2$ were carried out to seek favorable conditions for obtaining highly densified $NiFe_2O_4$ ceramic with extremely fine grain size.

During successful two-step sintering, the grain size should remain constant in the second-step sintering whereas density continues to increase, unlike in conventional sintering in which the final stage densification is invariably accompanied by rapid grain growth. Grain size-relative density trajectories of both CS and TSS are depicted in Fig. 6. It is clear that grain growth during the second-step sintering of TSS is suppressed. Additionally, it is hardly to obtain high density ceramics by mean of conventional sintering without sintering aids at comparable temperatures. For example, only 87.12%TD was obtained by conventional sintered $NiFe_2O_4$ compacts at 1150 °C for 15 h.

Table 1 lists some of the successful two-step sintering experiments. These experiments all achieved high density (≥98%TD) without obvious grain growth in the second step of TSS. In spite of the increase of relative density with the prolongation of holding time from 10 h to 20 h, the holding time of the second-step ($t_2$) is set as 15 h in the following TSS regimes, which stems from the negligible increase of relative density from 15 h to 20 h. Hence, the wasteful energy consumption can avoid. Meanwhile, it is observed that a higher $T_2$ for the same $T_1$ is mildly favorable to densify the specimens, though a slight grain growth (less than 10 nm in size) occurs. On the other hand, these experiments indicate that the lowest starting density, namely critical starting density, for the second-step sintering of TSS is approximately 81%TD, somewhat higher than for $Y_2O_3$ (about 75%TD) [6,15].

For $Y_2O_3$, there is a kinetic window expressed in grain size ($G_1$) and $T_2$ for the second-step sintering of TSS, within which high density without grain growth can be achieved as long as the starting density is above critical value [6,15]. Similar window determined for $NiFe_2O_4$ is delineated in Fig. 7, where

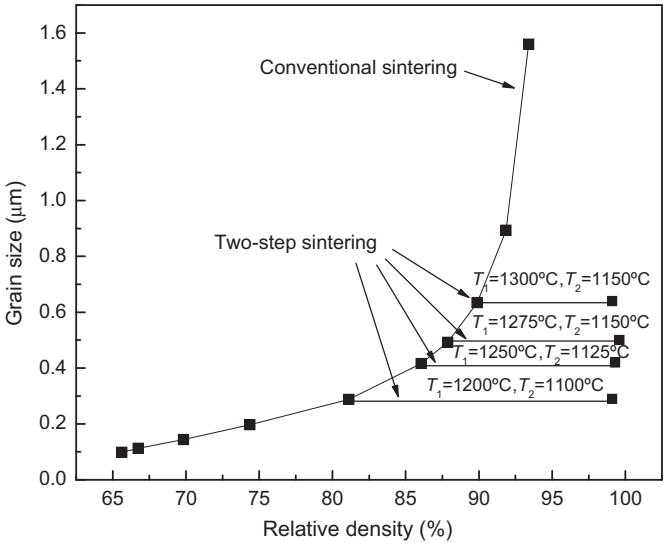


Fig. 6. Grain size versus relative density for specimens sintered by conventional sintering and two-step sintering.

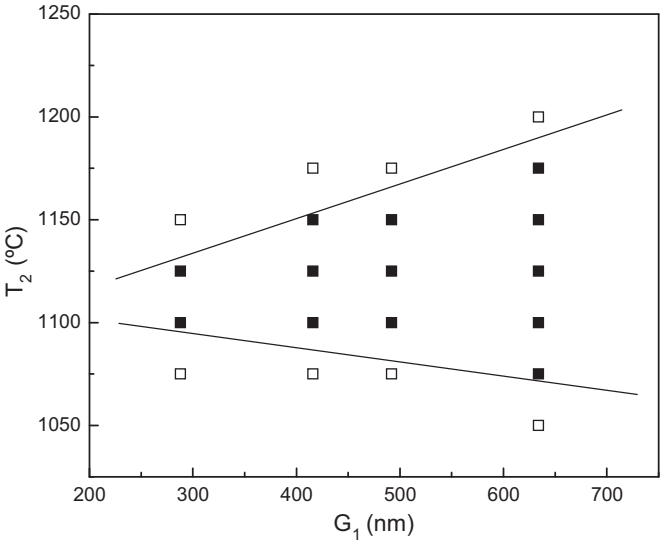


Fig. 7. Kinetic window for the second-step sintering of TSS without grain growth. Solid symbols are ones reaching high density without grain growth, open symbols are unsuccessful ones with either grain growth (upper) or poor density (lower).

solid symbols indicate samples successfully underwent the second-step sintering to reach high density without grain growth (as shown in Table 1). Open symbols below the lower boundary line are conditions that densification was exhausted despite no grain growth, and open symbols above the upper boundary line are ones in which grain growth occurred at $T_2$. In common with $Y_2O_3$, the slope of the upper boundary line is positive while the slope of the lower boundary line is negative, namely spanning a wider temperature range with increasing grain size. These similarities considerably imply similar mechanisms contributing in second-step sintering, even though the chemistry and crystal structures are various. The upper boundary is explained by the driving force for grain growth inversely proportional to grain size, so the temperature required for finer grain growth is lower. The lower boundary is interpreted by the threshold effect on interface kinetics. A threshold energy or stress could cause the suppression of grain boundary diffusion as long as its value is enough large caused by fine grain size. This effect diminishes with the increase of grain size, allowing the kinetic window to extend to lower temperatures for larger grain size.

Micrographs relating fracture surfaces of specimens sintered by two-step sintering and conventional sintering are shown in Fig. 8. It is obvious that the grain size after two-step sintering is extremely lower than that heated by conventional sintering. The finest grain size (290 nm) is that of the ceramic sintered at $T_1$ = 1200 °C and $T_2$ = 1100 °C (15 h) by TSS. In contrast, the coarsest grain size (2700 nm) is that of the sample densified by conventional sintering at 1250 °C for 5 h, whose corresponding density is 96.92%TD. For a further comparison, a sample was prepared by conventionally sintering the powders, deriving from solid-state interreaction between $Fe_2O_3$ and NiO, and its SEM micrograph is depicted in Fig. 8(f) with a grain size of about 7 μm (95.87%TD). These microstructure comparisons give powerful evidence on the superiorities of two-step sintering over other processing methods in obtaining high density ceramics with fine grains. Actually, it is the first time that such fine grain size is reported for nearly full dense $NiFe_2O_4$ ceramic.

### 3.4. Magnetic properties

Magnetic tests of the ceramics prepared by both two-step sintering and conventional sintering were performed by vibrating sample magnetometer at room temperature. The saturation magnetization ($M_S$), determined from the obtained hysteresis loops, as a function of grain size is sketched in Fig. 9, where solid and open square symbols stand for specimens obtained by two-step sintering and conventional sintering, as presented in Fig. 8, respectively. As shown in Fig. 9, the saturation magnetization is independent of grain size for nearly full samples obtained from two-step sintering, according with the result of high density NiCuZn ferrite prepared by TSS [16]. These values are around 54 emu/g, higher than that of the used $NiFe_2O_4$ nanopowder (46.5 emu/g, as shown in Fig. 9 using triangle). Lv et al. [4] reported that the $M_S$ value of $NiFe_2O_4$ ceramic with a mean grain size of 100 nm was 53 emu/g, in accordance with our aforementioned values. It shows that $NiFe_2O_4$ ceramics with fine grains possess likewise high saturation magnetization. In the same way, it indicates similar magnetization originating from indirect exchange interaction between tetrahedral and octahedral sublattices. The $M_S$ values of conventional sintered ceramics are somewhat lower than those of nearly full ceramics, owing to their higher porosities. The pores, both intragranular and intergranular, break exchange bonds between magnetic moment of anti-parallel spins. Therefore, the resultant magnetization would decrease.

### 3.5. Mechanical properties

The Vickers hardness and fracture toughness of specimens prepared under various conditions are shown in Table 2, where the samples (a)–(f) are obtained under the same condition as that of Fig. 8(a)–(f), respectively. As indicated by Table 2, the Vickers hardness increases with the decrease of grain size, which is similar to the tendency of fracture toughness. For the nearly full specimens prepared by TSS, the Vickers hardness and fracture toughness gradually increase with the decrease of grain size, indicating the grain size is the dominating factor. The highest Vickers hardness and fracture toughness, whose values are 8.47 GPa and 2.92 MPa $m^{1/2}$, respectively, are belonged to the specimen sintered by TSS with a grain size of 290 nm. Zhang et al. [32] reported that the values of Vickers hardness and fracture toughness of $NiFe_2O_4$-matrix cermet containing 20% (mass fraction) Cu–Ni mixed powders as toughening metallic phase were 3.81 GPa and 2.80 MPa $m^{1/2}$, respectively. These values are both lower than that of sample (a), especially for Vickers hardness. As shown in Fig. 8(a)–(d), the intergranular fracture is the common feature of all the specimens sintered by TSS, which indicates that the crack extents along grain boundary. The smaller the grain size is, the longer the crack propagation path is. Hence, the crack

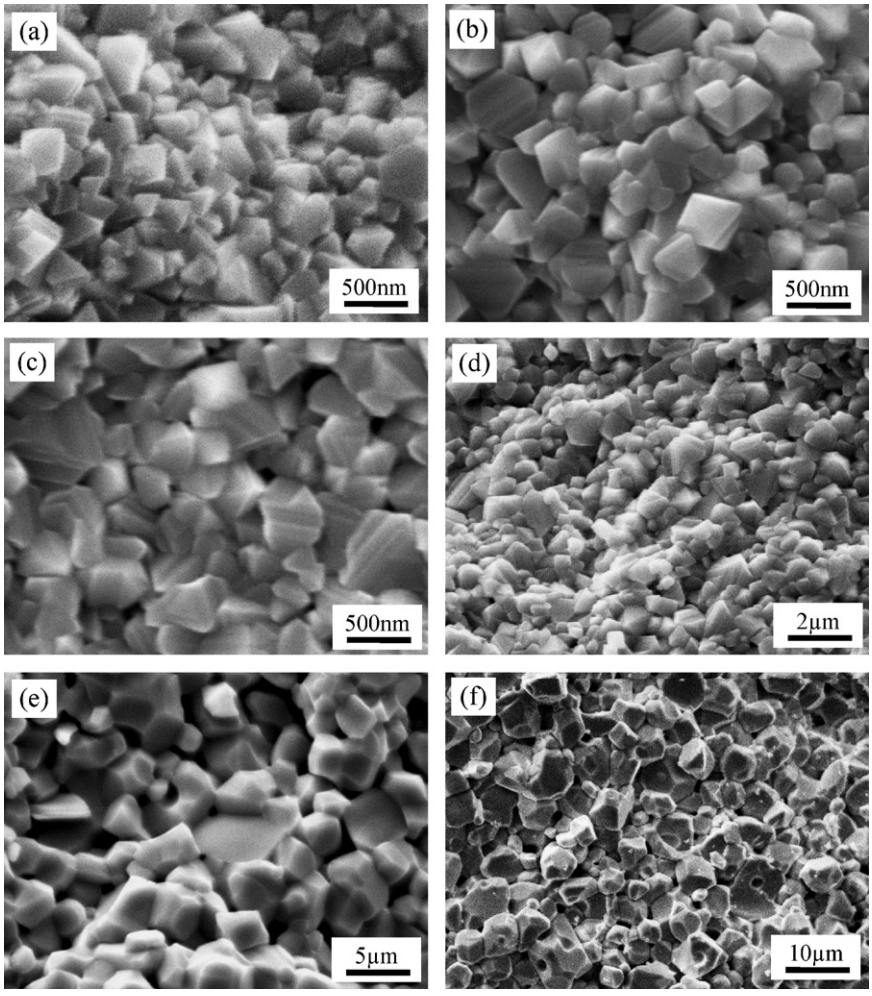


Fig. 8. SEM micrographs of dense $NiFe_2O_4$ ceramics prepared by two-step sintering: (a) 290 nm ($T_1$ = 1200 °C, $T_2$ = 1100 °C/15 h); (b) 420 nm ($T_1$ = 1250 °C, $T_2$ = 1125 °C/15 h); (c) 500 nm ($T_1$ = 1275 °C, $T_2$ = 1150 °C/15 h); (d) 640 nm ($T_1$ = 1300 °C, $T_2$ = 1150 °C/15 h); and conventional sintering (e) 2700 nm ($T$ = 1250 °C/5 h). (f) Sample conventionally sintered the powders from solid-state interreaction between $Fe_2O_3$ and NiO at 1250 °C for 5 h, 7 μm.

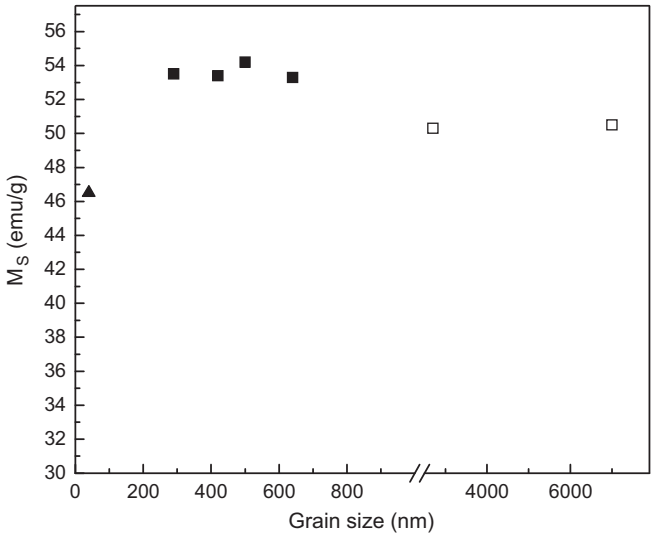


Fig. 9. Saturation magnetization ($M_S$) versus grain size for $NiFe_2O_4$ ceramics. Solid and open square symbols stand for specimens obtained by two-step sintering and conventional sintering, respectively. Triangle presents the $M_S$ value of the used $NiFe_2O_4$ nanopowder.

deflection is the predominant mechanism for higher toughness resulted in these samples. The conventional sintered samples, however, exhibit considerably lower Vickers hardness and fracture toughness values, attributing to the coarser grains and higher porosities. The decrease of Vickers hardness is associated with flaws of specimens such as pores and cracks. On the other hand, the decrease of the fracture energy dissipation resulting from flaws during the fracture process, together with the transgranular fracture (as presented in Fig. 8(e) and (f)), are both responsible for the decrease of

Table 2
Mechanical properties of $NiFe_2O_4$ ceramics prepared under various sintering conditions.

| Sample | Grain size (μm) | Relative density (%) | Vickers hardness (GPa) | Fracture toughness (MPa $m^{1/2}$) |
|---|---|---|---|---|
| a | 0.29 | 99.10 | 8.47 | 2.92 |
| b | 0.42 | 99.31 | 8.36 | 2.71 |
| c | 0.50 | 99.61 | 8.31 | 2.64 |
| d | 0.64 | 99.12 | 8.24 | 2.56 |
| e | 2.7 | 96.92 | 7.15 | 1.89 |
| f | 7.0 | 95.87 | 6.23 | 1.24 |

fracture toughness. These mechanical properties in this study indicate, therefore, that with the decrease of grain size via two-step sintering, not only does the hardness enhancement occur but also the fracture toughness increase.

## 4. Conclusions

To summarize, high density $NiFe_2O_4$ ceramics with fine grain size were successfully prepared by two-step sintering, suppressing accelerated grain growth in the final stage of sintering. The first-step sintering temperature $T_1$ should be set at the range of 1200–1300 °C due to its highest densification rate. In this temperature range, the intermediate density after $T_1$ is over critical value as well as the grain size is submicron. The kinetic window for achieving high density without grain growth in the second-step sintering of TSS has a characteristic shape, spanning a wider temperature range with increasing grain size. The saturation magnetization of nearly full $NiFe_2O_4$ ceramics is independent of grain size and likewise high, whose corresponding values are approximately 54 emu/g. The Vickers hardness and fracture toughness are both enhanced by decreasing the grain size and porosity. The highest values of Vickers hardness and fracture toughness are 8.47 GPa and 2.92 MPa $m^{1/2}$ for the nearly full $NiFe_2O_4$ ceramic with the finest grain size (290 nm), respectively. Therefore, the two-step sintering offers a promising approach for preparing nearly full ceramics with fine grain size in a simple way.

## Acknowledgments

Financial supports from the National Natural Science Foundation of China (Nos. 50834001 and 50971038) and the National High Technology Research and Development Program of China (No. 2009AA03Z502) are gratefully acknowledged.

## References

[1] C.J. Wang, C.Y. Huang, Y.C. Wu, Two-step sintering of fine alumina–zirconia ceramics, Ceram. Int. 35 (2009) 1467–1472.
[2] A. Muchtar, L.C. Lim, Indentation fracture toughness of high purity submicron alumina, Acta Mater. 46 (1998) 1683–1690.
[3] O. YT, J.B. Koo, K.J. Hong, J.S. Park, D.C. Shin, Effect of grain size on transmittance and mechanical strength of sintered alumina, Mater. Sci. Eng. A 374 (2004) 191–195.
[4] L. Lv, J.P. Zhou, Q. Liu, G.Q. Zhu, X.Z. Chen, X.B. Bian, P. Liu, Grain size effect on the dielectric and magnetic properties of $NiFe_2O_4$ ceramics, Physica E 43 (2011) 1798–1803.
[5] J.J. Sun, J.B. Li, G.L. Sun, W.G. Qu, Synthesis of dense NiZn ferrites by spark plasma sintering, Ceram. Int. 28 (2002) 855–858.
[6] I.W. Chen, X.H. Wang, Sintering dense nanocrystalline ceramics without final-stage grain growth, Nature 404 (2000) 168–171.
[7] D. Zhou, Y. Shi, J.J. Xie, Y.Y. Ren, P. Yun, Fabrication and luminescent properties of $Nd^{3+}$-doped $Lu_2O_3$ transparent ceramics by pressureless sintering, J. Am. Ceram. Soc. 92 (2009) 2182–2187.
[8] M. Pellizzari, A. Fedrizzi, M. Zadra, Influence of processing parameters and particle size on the properties of hot work and high speed tool steels by spark plasma sintering, Mater. Des. 32 (2011) 1796–1805.
[9] M. Omori, Sintering, consolidation, reaction and crystal growth by the spark plasma system (SPS), Mater. Sci. Eng. A 287 (2000) 183–188.
[10] W.L. Luan, L. Gao, H. Kawaoka, T. Sekino, K. Niihara, Fabrication and characteristics of fine-grained $BaTiO_3$ ceramics by spark plasma sintering, Ceram. Int. 30 (2004) 405–410.
[11] M. Hirano, M. Inagaki, Y. Mizutani, K. Nomura, M. Kawai, Y. Nakamura, Improvement of mechanical and electrical properties of scandia-doped zirconia ceramics by post-sintering with hot isostatic pressing, J. Am. Ceram. Soc. 83 (2000) 2619–2621.
[12] S. Ishihara, H. Gu, J. Bill, F. Aldinger, F. Wakai, Densification of precursor-derived Si–C–N ceramics by high-pressure hot isostatic pressing, J. Am. Ceram. Soc. 85 (2002) 1706–1712.
[13] D.j. Veljović, I. Zalite, E. Palcevskis, I. Smiciklas, R. Petrović, D.J. Janaćković, Microwave sintering of fine grained HAP and HAP/TCP bioceramics, Ceram. Int. 36 (2010) 595–603.
[14] E. Savary, S. Marinel, H. Colder, C. Harnois, F.X. Lefevre, R. Retoux, Microwave sintering of nano-sized ZnO synthesized by a liquid route, Powder Technol. 208 (2011) 521–525.
[15] X.H. Wang, P.L. Chen, I.W. Chen, Two-step sintering of ceramics with constant grain-size. I: $Y_2O_3$, J. Am. Ceram. Soc. 89 (2006) 431–437.
[16] X.H. Wang, X.Y. Deng, H.L. Bai, H. Zhou, W.G. Qu, L.T. Li, I.W. Chen, Two-step sintering of ceramics with constant grain-size. II: $BaTiO_3$ and Ni–Cu–Zn ferrite, J. Am. Ceram. Soc. 89 (2006) 438–443.
[17] H.T. Kim, Y.H. Han, Sintering of nanocrystalline $BaTiO_3$, Ceram. Int. 30 (2004) 1719–1723.
[18] M. Mazaheri, A.M. Zahedi, S.K. Sadrnezhaad, Two-step sintering of nanocrystalline ZnO compacts: effect of temperature on densification and grain growth, J. Am. Ceram. Soc. 91 (2008) 56–63.
[19] P. Durán, F. Capel, J. Tartaj, C. Moure, A strategic two-stage low-temperature thermal processing leading to fully dense and fine-grained doped-ZnO varistors, Adv. Mater. 14 (2002) 137–141.
[20] M. Mazaheri, A. Simchi, F.G. Fard, Densification and grain growth of nanocrystalline 3Y-TZP during two-step sintering, J. Eur. Ceram. Soc. 28 (2008) 2933–2939.
[21] K. Bodišová, P. Šajgalík, D. Galusek, P. Švančárek, Two-stage sintering of alumina with submicrometer grain size, J. Am. Ceram. Soc. 90 (2007) 330–332.
[22] M. Mazaheri, A.M. Zahedi, M. Haghighatzadeh, S.K. Sadrnezhaad, Sintering of titania nanoceramic: densification and grain growth, Ceram. Int. 35 (2009) 685–691.
[23] Y.I. Lee, Y.W. Kim, M. Mitomo, Fabrication of dense nanostructured silicon carbide ceramics through two-step sintering, J. Am. Ceram. Soc. 86 (2003) 1803–1805.
[24] R.H. Kodama, Magnetic nanoparticles, J. Magn. Magn. Mater. 200 (1999) 359–372.
[25] H. Kavas, A. Baykal, M.S. Toprak, Y. Köseoğlu, M. Sertkol, B. Aktaş, Cation distribution and magnetic properties of Zn doped $NiFe_2O_4$ nanoparticles synthesized by PEG-assisted hydrothermal route, J. Alloys Compd. 479 (2009) 49–55.
[26] E. Olsen, J. Thonstad, Nickel ferrite as inert anodes in aluminium electrolysis. Part I: material fabrication and preliminary testing, J. Appl. Electrochem. 29 (1999) 293–299.
[27] E. Olsen, J. Thonstad, Nickel ferrite as inert anodes in aluminium electrolysis. Part II: material performance and long-term testing, J. Appl. Electrochem. 29 (1999) 301–311.
[28] H.P. Klug, L.E. Alexander, X-ray Diffraction Procedure, fourth ed., Wiley, New York, 1954.
[29] J.B. Wachtman, Mechanical Properties of Ceramics, first ed., Wiley, New York, 1996.
[30] G.R. Anstis, P. Chantikul, B.R. Lawn, D.B. Marshall, A critical evaluation of indentation techniques for measuring fracture toughness. I: direct crack measurements, J. Am. Ceram. Soc. 64 (1981) 533–543.
[31] J.D. Hansen, R.P. Rusin, M.H. Teng, D.L. Johnson, Combined stage sintering model, J. Am. Ceram. Soc. 75 (1992) 1129–1135.
[32] G. Zhang, J. Li, Y.Q. Lai, Z.L. Tian, Effect of metallic phase content on mechanical properties of (85Cu–15Ni)/(10NiO–$NiFe_2O_4$) cermet inert anode for aluminum electrolysis, Trans. Nonferrous Met. Soc. China 17 (2007) 1063–1068.